HHS Public Access

Author manuscript

Ann Biomed Eng. Author manuscript; available in PMC 2017 November 01.

Published in final edited form as:

Ann Biomed Eng. 2016 November ; 44(11): 3202–3214. doi:10.1007/s10439-016-1602-x.

Accuracy of 4D Flow measurement of cerebrospinal fluid dynamics in the cervical spine: An in vitro verification against numerical simulation

Soroush Heidari Pahlavian[1,2], **Alexander C. Bunck**[3,4], **Suraj Thyagaraj**[1,2], **Daniel Giese**[3], **Francis Loth**[1,2], **Dennis M. Hedderich**[3], **Jan Robert Kröger**[4], and **Bryn A. Martin**[5]

[1]Conquer Chiari Research Center, The University of Akron, Akron, OH, U.S.A.

[2]Department of Mechanical Engineering, The University of Akron, Akron, OH, U.S.A.

[3]Department of Radiology, University Hospital of Cologne, Cologne, Germany

[4]Department of Radiology, University Hospital of Muenster, Muenster, Germany

[5]Department of Biological Engineering, The University of Idaho, Idaho, USA

Abstract

Abnormal alterations in cerebrospinal fluid (CSF) flow are thought to play an important role in pathophysiology of various craniospinal disorders such as hydrocephalus and Chiari malformation. Three directional phase contrast MRI (4D Flow) has been proposed as one method for quantification of the CSF dynamics in healthy and disease states, but prior to further implementation of this technique, its accuracy in measuring CSF velocity magnitude and distribution must be evaluated. In this study, an MR-compatible experimental platform was developed based on an anatomically detailed 3D printed model of the cervical subarachnoid space and subject specific flow boundary conditions. Accuracy of 4D Flow measurements was assessed by comparison of CSF velocities obtained within the *in vitro* model with the numerically predicted velocities calculated from a spatially averaged computational fluid dynamics (CFD) model based on the same geometry and flow boundary conditions. Good agreement was observed between CFD and 4D Flow in terms of spatial distribution and peak magnitude of through-plane velocities with an average difference of 7.5% and 10.6% for peak systolic and diastolic velocities, respectively. Regression analysis showed lower accuracy of 4D Flow measurement at the timeframes corresponding to low CSF flow rate and poor correlation between CFD and 4D Flow in-plane velocities.

Keywords

Magnetic resonance imaging; 4D Flow measurement; Cerebrospinal fluid; Computational fluid dynamics; Phantom experiment

CORRESPONDING AUTHOR: Bryn A. Martin, 875 Perimeter Drive MS 0904, Moscow, ID 83844-0904, Tel: +1 (208)885-1030, brynm@uidaho.edu.

Conflict of interest

Authors have no conflict of interests.

1 INTRODUCTION

Cerebrospinal fluid (CSF) serves many important roles in the central nervous system (CNS) including structural protection[21], metabolic homeostasis, and immunological support[19, 22]. Abnormal CSF production, absorption, and/or dynamics are thought to play an important role in several CNS disorders such as Alzheimer's disease[33, 38], hydrocephalus[4], Chiari malformation[5], and Syringomyelia[10, 26]. CSF has also been investigated as a transport route and medium for delivery of therapeutic molecules to neuronal and glial cells of CNS tissues[32, 34]. As such, a better understanding of CSF dynamics can improve the diagnosis and treatment of CNS disorders. Numerous studies have been carried out to assess CSF dynamics in the spinal subarachnoid space (SAS) using *in vivo* measurement techniques such as phase contrast magnetic resonance imaging (PCMRI)[24] and intraoperative ultrasound. More recently, the development of time-resolved three directional PCMRI sequences (4D Flow) has enabled the simultaneous measurement of velocities in through-plane and in-plane directions and allows for higher spatio-temporal resolution compared with conventional 2D PCMRI methods within a clinically feasible time-frame[5, 35]. Researchers have applied 4D Flow to investigate *in vivo* CSF velocity magnitudes and distribution in the spinal SAS[5, 14]. Due to its high spatio-temporal resolution and its ability to measure velocity components corresponding to secondary flows, 4D Flow has the potential for many clinical applications such as diagnostic measurements and prediction of intrathecal drug distribution. However, prior to further implementation of this technique, validation studies are needed to verify the accuracy of the obtained measurements.

The goal of the present study was to investigate the accuracy of 4D Flow measurements of CSF in terms of velocity magnitude and distribution. Our approach was to assess 4D Flow accuracy by comparing CSF velocities obtained from an *in vitro* subject-specific model of cervical SAS with numerically predicted velocities obtained from a spatially averaged computational fluid dynamics (CFD) model based on the same geometry and boundary conditions.

2 MATERIALS AND METHODS

2.1 Ethics Statement

The MRI data acquisition of the adult healthy volunteer was performed at the Department of Radiology of Munster. The study was approved by the institutional review board of the University of Munster. Prior to completion of the MRI exams, written informed consent was obtained from the volunteer and the obtained data were anonymized before further processing.

2.2 Subject-specific model of cervical SAS

MRI data acquisition was performed as previously described[15]. In brief, a three dimensional turbo spin-echo sequence was used to obtain T2-weighted MRI images of the cervical spine with an isotropic spatial resolution of 0.8 mm. The three-dimensional geometry of cervical SAS, containing dura mater layer and spinal cord was reconstructed from the manual segmentation of MRI images using ITK Snap[41] (version 2.2, University of Pennsylvania,

Philadelphia, Pennsylvania, USA) (Figure 1 a). The geometry was segmented ~5 cm caudal to the last cervical vertebra to reduce entrance length effects and the resulting surface model was smoothed to remove the pixilation artifacts.

In order to increase the anatomical fidelity of the model, idealized 3D spinal nerve rootlets were designed and added to the segmented geometry at each level along the spine using Autodesk Maya (version 2014, Autodesk Inc., Mill Valley, CA) based on the ex-vivo measurements available in the literature[1] (Figure 1 b). A more detailed modeling process of these fine structures and their corresponding dimensions is described in a previous work[15]. Note that in the present study, nerve rootlets were designed with a minimum thickness of 1 mm in order to meet the constraint imposed by the resolution of the 3D printer. The 3D printer limitation also made it impractical to include other fine anatomical features (i.e. denticulate ligaments) and thus these structures were not modeled in the current geometry. In order to make the model suitable for 3D printing, a hollow geometry was created by Boolean subtraction of the model from a rectangular cuboid (Figure 1 c). The final composite models were inspected for topological inconsistencies using Geomagic Studio (3D System Corp., Valencia, CA) and exported as an STL files suitable for CFD grid generation and 3D printing.

2.3 Bench-top experimental model

The composite geometry of the cervical SAS, including idealized nerve rootlets, was used to construct a phantom model (Figure 1 c) out of photo-reactive resin (Watershed XC 11122, DSM Somos Corp., Elgin, IL) using a stereolithography technique[20] (Viper si2 SLA system, 3D System Corp., Valencia, CA). The 3D printer layer thickness was 101.6 μm and the model was rigid and included additional extensions to provide necessary space for the flow system fittings.

The fluid used for the *in vitro* experiment was water, since its rheological properties is considered to be close to those of CSF[3]. A representative flow waveform with similar shape to that obtained *in vivo* was used for the experiment. The amplitude of the flow waveform was modulated so that the peak CSF velocities obtained from the *in vitro* experiment fall in the range observed by *in vivo* PC-MRI measurements[5, 14]. Each CSF flow pulsation created a stroke volume of ~1.8 cm^3 with a maximum systolic and diastolic flow rate of 10.0 cm^3/s and 6.5 cm^3/s in the craniocaudal and caudocranial directions, respectively.

The phantom model was placed within a flow system consisting of a computer-controlled pulsatile syringe pump, which simulated the desired CSF flow waveform[26]. The pulsatile pump consisted of a 3 ml precision glass syringe which was moved in a pulsatile manner by a tubular linear servo motor (TT Micro Model #TB1106, Copley Controls Corp., Canton, MA) according to a voltage signal generated by a laptop computer. Low viscosity spindle oil was used to lubricate the syringe shaft during the operation and a custom designed oil-water boundary cylinder was used to separate the syringe from the water entering the flow model. The pump was connected to the 3D printed model through a 7.6 m long, 6.4 mm ID rigid plastic tube. The use of this long tubing was necessary to keep all metallic components of the flow system away from the MRI scanner. The tubing that connected the pump and model

was held in place to a solid surface at several locations by adhesive to minimize waveform degradation due to tubing motion.

2.4 4D Flow in vitro measurements

In vitro 4D Flow measurements were performed based on a previously detailed protocol[5]. In brief, a 1.5 T MRI (Achieva, Philips Healthcare, Best, Netherlands) equipped with a 16-channel head and neck coil was used and 4D Flow measurements were obtained from a retrospectively ECG triggered, gradient and RF spoiled, T1-weighted, segmented gradient echo sequence with acquired in plane and through-plane resolutions of 1.0 and 1.5 mm, respectively. Sequence parameters were as follows: Repetition time (TR) and Echo time (TE) was set to "shortest" resulting in a TR of 8.9 ms and a TE of 5.7 ms, flip angle: 5°. Images were collected in the sagittal orientation and flow velocities were encoded in anterior-posterior, in feet-head and in right-left directions. The encoding velocity (V_{ENC}) was set to 15 cm/s for all direction and the cardiac cycle was temporally encoded in 16 phases, corresponding to an acquired temporal resolution of 52ms. 4D Flow data was corrected for concomitant field induced phase offsets[2]. GTFlow software (version 2.2.6, Gyrotools Ltd., Zurich, Switzerland) was used for the post-processing of 4D Flow data including the correction for eddy current induced phase offsets[37] and aliasing artifacts. The *in vitro* model was submerged in a water bath during the scan and the surrounding water was considered as the static tissue for the eddy currents phase offsets corrections. Through-plane and in-plane velocities were obtained at eight different axial planes and exported as data files for further analysis and comparison with CFD results.

2.5 Numerical flow simulation

The composite geometry STL file was imported into ICEM CFD software (version 15.0, ANSYS Inc., Canonsburg, PA) and was discretized into a nonuniform unstructured rigid-walled computational grid with 12 million elements (Figure 1 d). Grid refinement near the walls and nerve rootlets was used to accurately capture the larger gradients in these regions.

CFD simulation was carried out using ANSYS FLUENT (version 15.0, ANSYS Inc., Canonsburg, PA) and based on the methodology and setup described previously[15]. In brief, CSF was considered to be an incompressible Newtonian fluid and its rheological properties were assumed to be the same as those of water at the temperature during the *in vitro* experiments (26 °C) and its flow was assumed to be laminar. 4D Flow was chosen to obtain CFD boundary condition based on flow rates measured at eight axial planes, due to its significantly shorter scan time compared to traditional 2D PCMRI techniques. An inlet velocity profile based on the average of these measured flow rates was imposed on the cranial end of the geometry. Two hundred time-steps per cycle were computed for the simulation and results are presented based on the third flow cycle to minimize startup effects. Independence studies were performed for grid size, time-step size, and periodicity and described in the Supplementary Material.

While a detailed analysis of the CSF flow filed is possible by using CFD simulations due to their high spatial and temporal resolution, current clinically oriented 4D Flow measurement techniques are limited by their resolution, which is an order of magnitude lower than that of

CFD. As such, a high resolution CFD simulation may produce some flow features that are undetectable by 4D Flow. This required averaging of the CFD simulation results for accurate comparison to the 4D Flow measurements.

The 4D Flow post-processing software used in the present study, GTFlow, linearly interpolated the raw MRI data onto a grid finer than the original voxel acquisition size. Interpolation of the 4D Flow output data was required to allow flow data analysis in any desired orientation within the flow field. Thus, the CFD results were spatially averaged to the original MR voxel resolution (1.5 and 1.0 mm through-plane and in-plane resolution, respectively) and then upsampled to the GTFlow software output resolution (0.49 mm isotropic). Post-processing of CFD results were carried out using an in-house code as shown in Figure 2.

2.6 Analysis and Comparison Method

For the qualitative and quantitative comparison of *in vitro* measurements and averaged CFD results, three-directional velocities were extracted at eight axial planes throughout the geometry. These axial planes were manually positioned in the space between foramen magnum (FM) and the midline of the seventh cervical vertebral bone (C7). An in-house code using MATLAB (MATLAB, MathWorks, Natick, MA) was employed to quantify and compare CSF dynamics obtained from CFD and *in vitro* 4D Flow within individual axial planes. Quantified parameters included CSF flow rate, velocity distributions, and peak velocity magnitudes.

More detailed comparison between simulation and *in vitro* experiment was made possible by performing a correlation analysis of local through-plane and in-plane CSF velocities between averaged CFD results and *in vitro* 4D Flow measurements. Pixel by pixel comparison of velocity component between CFD and 4D Flow at each axial plane was completed by matching the relative position of the corresponding structural images using a two-dimensional translational cross-correlation technique in MATLAB (xcorr2). For each pixel, the value of the local CFD velocity was plotted against the corresponding value obtained from 4D Flow measurement and linear regression analysis was performed for all axial planes and timeframes.

3 Results

3.1 4D Flow measured flow rate variability

CSF flow rate was quantified from in-vitro 4D Flow measurements at eight different axial planes during the cardiac cycle with a typical systolic and diastolic peak flow rate of 12.0 and 7.0 ml/s, respectively. The waveform shape was maintained by each axial plane as expected with an average standard deviation of 0.36 ml/s over all timeframes (Figure 3). While the agreement among different axial planes was relatively good, a maximum difference of 18% was observed between waveforms measured at FM and C5 axial planes at peak systole. A similar trend was observed for the standard deviation of flow rate with the maximum of 0.79 ml/s measured at peak systole.

3.2 Qualitative comparison of velocity patterns

Figure 4 compares the surface plots of the through-plane velocities obtained from CFD and *in vitro* 4D Flow at peak systole and peak diastole. Note that Figure 4 color scales are varied for each axial plane to maximize the details shown. Good agreement was observed in terms of spatial distribution and peak magnitude of through-plane velocities. Both the *in vitro* and CFD results showed anterior dominance of the CSF flow in the axial planes near the cranial end of the geometry (C1 and C2) and also regions of elevated flow between nerve rootlets, albeit these flow features were more pronounced in the simulation results.

Some differences were observed between the profile shapes obtained from CFD simulation and *in vitro* measurements which were more pronounced at the axial planes near the cranial end of the geometry and also near the edges of the axial planes and the nerve rootlets (red arrows in Figure 4). Despite the overall qualitative agreement in velocity distributions, the exact in-plane location of distinct peak velocity values (e.g. jets) varied between the CFD and *in vitro* results. The maximum spatial distance of these peak velocity values in the CFD and *in vitro* results ranged up to 15 mm in distance within each plane. Also, spatial and temporal velocity variations with a magnitude of ~1-2 cm/s were observed at some locations in 4D Flow velocity profiles that were not observed in CFD results.

The discrepancy of in-plane velocities was much greater than that of the through-plane velocities. Figure 5 compares the in-plane velocity vectors obtained from CFD and *in vitro* measurements on a representative axial plane (C1). A significant difference was observed in in-plane velocity magnitudes and directions, as 4D Flow in-plane velocities pointed in different directions and appeared to lack the coherence seen in CFD results. Also, secondary flow features, such as vortices, occurred in one data set but not in the other.

3.3 Quantitative comparison of velocities

A detailed quantitative comparison between *in vitro* and CFD results was performed at the axial planes over the cardiac cycle. Figure 6 illustrates the comparison of peak CSF velocities obtained from CFD simulation and *in vitro* measurements for all axial planes at peak systole and diastole. A good agreement was observed between CFD and 4D Flow peak CSF velocities at different axial planes. Average difference over all planes for peak systolic and diastolic CSF velocities between CFD and 4D Flow was 0.85±0.79 and 0.73±0.39 cm/s, respectively with a maximum difference of 36% that occurred at the FM at peak diastole. Larger discrepancies in CSF velocities were observed at timeframes when flow rate was nearly zero (up to 150%, not shown in Figure 6).

Differences between through-plane velocities obtained from *in vitro* 4D Flow and CFD were further quantified using Bland-Altman plots as shown in Figure 7. The results shown in Figure 7 correspond to all cardiac timeframes and are plotted for the axial planes with highest and lowest correlation coefficient between CFD and 4D Flow through-plane velocities (C3 and FM, respectively). Close correlation was observed from the linear regression analysis in both planes ($r = 0.81$ and 0.93 for FM and C3, respectively), although the correlation at the FM proved to be less favorable, evident from its lower r and slope values. The second set of Bland-Altman plots showed that the value of discrepancy between

CFD and *in vitro* results can be higher for greater CSF velocities and that the 95% confidence intervals were limited by 1.2-1.8 cm/s velocities, similar to the values seen for the random fluctuations of 4D Flow velocities mentioned above.

The results of the linear regression analysis averaged over all axial planes are summarized in Figure 8 a, which shows the calculated slopes and correlation coefficient as a function of timeframes. Good correlation of 4D Flow measurements and CFD results (r>0.75) was observed at most of the timeframes. Higher values of mean correlation coefficient and mean slope were measured near peak systole (timeframe 8), while a large standard deviation in slope and weaker correlation between CFD and 4D Flow velocities were observed at the timeframes corresponding to near zero CSF flow rate (CSF flow reversal at timeframes 6 and 12 in Figure 8 a).

Figure 8 b depicts the variation of mean slopes and correlation coefficients averaged over all timeframes as a function of axial location. Overall, good correlation was observed between 4D Flow and CFD. However, the mean slopes and correlation coefficients were lower in the axial planes near the cranial end of the geometry (Figure 8 b). This is reflected by the increased mismatch of CFD and *in vitro* results at the cranial region. Also, the mean slope values were consistently below unity in both Figures 8 a and b, indicating a tendency of CFD simulations to overestimate the CSF velocities measured by 4D Flow.

As expected from the qualitative comparison of in-plane velocities, poor correlation coefficients were calculated from the linear regression analysis of in-plane velocities obtained from CFD and 4D Flow. The maximum values of mean correlation coefficients averaged over all axial planes and all timeframes were 0.52±0.19 and 0.50±0.10 that was measured at the 9th timeframe and C8 axial plane, respectively.

3.4 Impact of spatial averaging on the Numerical results

Figure 9 depicts the variability in CFD peak through-plane velocity contours for a representative axial plane over a distance of 1.0 mm, which is equivalent to the through-plane slice thickness of 4D Flow measurements. Despite having a similar range of magnitude, velocity distribution patterns showed some alteration, especially near the regions with greater geometrical variation (near nerve rootlets). These alterations highlight the need for spatial averaging of the CFD results before comparison with 4D Flow and also the added flow detail that CFD can provide. As shown in Figure 9, averaging of CFD velocities decreased peak through-plane velocity magnitude up to 25%. Also, some flow features such as anterolateral dominance of the flow and concentrated flow regions between nerve rootlets were weakened or completely diminished as a result of averaging.

4 Discussion

Quantitative assessment of CSF dynamics is thought to be important because of its potential application to help characterize CNS disorders such as Chiari malformation[5, 6, 10], predict CSF pressure gradients[13] and predict intrathecal drug distribution[17]. *In vivo* 4D Flow assessment of CSF hydrodynamics is desirable because all velocity components can be directly obtained; whereas, MRI-based CFD techniques require a number of assumptions

and simplifications. However, before reaching a broad clinical use, the accuracy of 4D Flow measurement of CSF velocities must be verified. To assess accuracy, our approach was to construct and test an anatomically realistic *in vitro* model of the cervical SAS and verify the results against numerical simulations. Construction and testing of the anatomically realistic *in vitro* model, as a means for comparison of the CFD and 4D Flow measurements, allowed control of the geometry and flow boundary conditions that is not possible with *in vivo* measurements. Herein, our discussion focuses on qualitative and quantitative comparison of thru-plane and secondary velocity results and highlights the possible sources of error due to the 4D Flow and CFD post-processing methods.

4.1 Agreement of thru-plane CSF velocities

Our findings showed a good qualitative and quantitative agreement between numerical simulations and *in vitro* 4D Flow measurements in terms of through-plane velocities (Figure 4). Albeit, the magnitude of thru-plane peak velocities was generally greater in the CFD results compared to 4D Flow (Figure 6). The comparison of through-plane velocity profile shapes revealed similar flow characteristics, as the overall velocity distribution and also more distinctive flow features, such as anterior dominance of flow and anterolateral jets, were detected by both techniques (Figure 4). Quantitative comparison of CFD and *in vitro* data yielded a close correlation of through-plane velocities at most axial planes and timeframes (Figure 8). The correlation was particularly strong at the timeframes corresponding to peak systolic and diastolic CSF flow and at axial locations with greater CSF velocities.

In previous assessments of CSF velocities using *in vivo* 4D Flow measurements, large discrepancies were reported between *in vivo* 4D Flow and MRI-based CFD models in terms of velocity magnitude and distribution at peak systole [39]. For example, Yiallourou et al. [39] and Pahlavian et al. [31] reported a large difference between peak CSF velocities measured by 4D Flow and calculated from CFD in healthy volunteers (up to 300%) and patients diagnosed with Chiari malformation (up to 600%). Also, a substantial difference was reported in velocity distributions measured by 4D Flow and predicted by CFD, characterized by more pronounced anterior and anterolateral dominance of the flow in *in vivo* measurements. The reported differences between CFD and *in vivo* measurements were located at high CSF velocity regions. Thus, the present study results support that the previous *in vivo* 4D Flow measurements were likely correct and that the differences in CFD results were due to modeling simplification and/or assumptions such as the SAS geometry and absence of compliance and/or porosity in the model. These differences were not likely to be due to operator segmentation error[27].

Despite the general good agreement between CFD and *in vitro* results, some discrepancies were observed in the through-plane velocities obtained from these methods. In terms of overall velocity distribution, a greater mismatch between CFD and *in vitro* results was observed on axial planes closer to the cranial end of the geometry (Figure 4). Also, a weaker correlation between CFD and *in vitro* through-plane velocities was observed at planes near the cranial end of the geometry (Figure 8 b). One possible reason for this could be the lower velocity to noise ratio (VNR) of 4D Flow measurements at these planes due to their larger

cross-sectional area and lower velocities. A high value of the V_{ENC} parameter produces low VNR in the low velocity flow regions and the detailed flow structures cannot be resolved precisely in these regions[12]. In the present study a V_{ENC} value of 15 cm/s was used, yet the peak velocities at axial planes near the cranium were much lower at 6-8 cm/s. Also, local velocities at these planes were as low as 1 cm/s in a relatively large portion of the area (see posterior side of FM and C1 during diastole in Figure 4). This limitation in 4D Flow measurements can also explain the weak correlation between CFD and *in vitro* through-plane velocities at the timeframes close to CSF flow reversal (near zero flow rate). The precision of 4D Flow can be enhanced for measuring lower velocities by using a multiple V_{ENC} sequences[12] and/or using a time-dependent V_{ENC}. Furthermore, detailed comparison of through-plane velocity profile shapes revealed regions with local discrepancies, which were mainly located near the nerve rootlets (red arrows in Figure 4). The other difference observed in velocity patterns was the spatiotemporal velocity fluctuations in 4D Flow results which were not present in CFD velocities. The exact cause of these fluctuations is unclear, but 4D Flow measurement artefacts and noise could have contributed to their formation.

4.2 Poor similarity of secondary flow components

Our results show that measured in-plane 4D Flow velocities are not accurate in the current geometry. The in-plane velocities obtained from 4D Flow showed a high degree of noise and incoherence in comparison to CFD (Figure 5). These discrepancies are mainly the result of the 4D Flow error due to the low in-plane velocity magnitudes and were observed in previous studies of blood flow measurements[23]. As such, improvement of 4D Flow sequences through implementation of lower V_{ENC} for in-plane velocities or multiple V_{ENC} acquisitions should be performed prior to further consideration of this technique for quantification of secondary flow components. Secondary components of CSF flow can have an important impact on its mixing characteristics and could be used to enhance the prediction of intrathecal drug distribution[15, 18, 29, 32].

4.3 Lack of consistency in 4D Flow measured CSF flow waveforms

Despite using a rigid phantom model, axial variations were observed in the 4D Flow-measured volumetric CSF flow rate throughout the geometry (Figure 3). A maximum difference of 18% was measured between FM and C5 axial planes at the timeframe corresponding to peak CSF flow rate. Similar discrepancies in PCMRI-measured flows were reported in previous *in vitro* assessment of blood velocities[23, 28], albeit with lower error of 5-6%.

The observed variation could be caused by 4D Flow measurement error and post-processing. In the present study, 4D Flow data underwent a linear eddy current correction. Although 1st order eddy-current corrections have been performed on the 4D Flow measurements, remaining errors are likely due to phase offsets not correctible by the eddy current correction algorithm. These include higher order eddy currents but also eddy-current variations throughout the segmented acquisition due to steady-state loss and/or temperature variations of the gradient system[11]. Another source of error that remains in the 4D Flow data that could explain the higher velocity discrepancies at the field of view edges are gradient field distortions and their effect on the V_{ENC}[25]. One approach for reducing the aforementioned

errors is the incorporation of recently developed divergence-free de-noising processing techniques[8, 30], which enforce physical constraint of fluid incompressibility to the measured flow field. These noise reduction features were not available in the post-processing software used in the current study.

The axial variation of CSF flow rate along cervical SAS was previously reported in *in vivo* PCMRI studies and its presence was postulated to be indicative of SAS compliance[14, 40]. The presence of CSF flow variations along the rigid *in vitro* model, with exactly the same flow waveform present throughout the model, revealed that SAS compliance may not be the sole reason behind this phenomenon and it could be, in part, due to an artifact of 4D Flow error.

4.4 Importance of post-processing and limitations of CFD and experimental methods

An important methodological aspect of the present study was the post-processing and spatial averaging of CFD data prior to their comparison with 4D Flow measurements. Our results demonstrate that velocity distribution details are diminished as a result of the spatial averaging that is necessary to obtain 4D Flow data (Figure 9). In particular, spatial averaging resulted in up to a 25% reduction in peak CSF velocities. This result indicates that the peak in vivo CSF velocities detected by 4D Flow in previous studies[6, 7, 39] could be substantially greater than realized. Future improvement of 4D Flow sequences are needed for enhancing its spatial and temporal resolution, particularly for situations where it is critical to quantify highly resolved flow patterns.

The CFD simulation conducted in this study had a number of limitations. For the flow boundary condition, we applied a CSF flow rate detected by 4D Flow (Figure 3). This methodology was applied in a number of previous *in vitro* MRI studies in the literature[9, 23]. The CFD simulations were performed using a laminar flow assumption. The maximum Reynolds number, based on internal flow, was calculated to be 960. Thus, it is possible that some local transitional flow features were present in the *in vitro* model[16]. Additional experimental measurements of parameters such as flow rate and pressure gradient would further describe the flow field inside the in vitro model. However, these measurements are difficult to perform accurately due to the small amplitudes of both flow and pressure gradient waveforms. Also, 4D Flow measurements are phase-averaged and thus do not allow quantification of high-frequency velocity fluctuations that may be present in the CSF flow. Emerging works pertaining to real-time phase-contrast MRI[36] might prove to be useful in detection of these velocity fluctuations.

Although the 3D printing layer thickness of 101.6 μm was smaller than the segmentation resolution (800 μm), it still resulted in non-smooth surfaces in the constructed model, which were not present in the geometry used in the CFD model. This surface roughness is expected to have a minor impact on the measured velocities, due to its small size and the relatively low Reynolds number of CSF flow. Controlled treatment of the constructed geometry using *abrasive flow deburring* might be useful to minimize the impact of the surface roughness created during the 3D printing process. However, such techniques have the risk of altering the geometry beyond roughness correction.

Additional experimental measurements of parameters such as flow rates and pressure gradient can lead to a more accurate representation of the CSF flow field inside the *in vitro* model. However, due to the small amplitudes of the flow rate and pressure gradient waveforms, such measurements are difficult to perform on the model used in the current study.

5 Conclusion

The accuracy of 4D Flow detection of CSF dynamics in the cervical spine was assessed by usage of an *in vitro* model and comparison to numerical simulations. 4D Flow was found to accurately measure through-plane CSF velocities and distribution throughout the cervical SAS at timeframes near peak systolic and diastolic CSF flow rates. In-plane assessment of CSF velocities and CSF velocities at low flow rates (e.g. near flow reversal) were not found to be accurate. These results support the use of 4D Flow to assess CSF velocities as an indicator of CNS disease states.

Supplementary Material

Refer to Web version on PubMed Central for supplementary material.

Acknowledgments

Authors would like to appreciate Conquer Chiari and American Syringomyelia Alliance Project for the support of this work. Authors would also like to acknowledge Dr. Jae-Won Choi and Dr. Morteza Vatani for the helpful discussions and assistance in the rapid-prototyping of the phantom model.

Abbreviations

CSF	cerebrospinal fluid
CNS	central nervous system
SAS	subarachnoid space
PCMRI	phase-contrast magnetic resonance imaging
CFD	computational fluid dynamics
FM	foramen magnum
TR	repetition time
TE	echo time
VENC	encoding velocity
VNR	velocity to noise ratio

References

1. Alleyne CH Jr. Cawley CM, Barrow DL, Bonner GD. Microsurgical anatomy of the dorsal cervical nerve roots and the cervical dorsal root ganglion/ventral root complexes. Surg Neurol. 1998; 50:213–218. [PubMed: 9736081]
2. Bernstein MA, Zhou XJ, Polzin JA, King KF, Ganin A, Pelc NJ, Glover GH. Concomitant gradient terms in phase contrast MR: analysis and correction. Magnetic Resonance in Medicine. 1998; 39:300–308. [PubMed: 9469714]
3. Bloomfield IG, Johnston IH, Bilston LE. Effects of proteins, blood cells and glucose on the viscosity of cerebrospinal fluid. Pediatr Neurosurg. 1998; 28:246–251. [PubMed: 9732257]
4. Bradley WG Jr. Scalzo D, Queralt J, Nitz WN, Atkinson DJ, Wong P. Normal-pressure hydrocephalus: evaluation with cerebrospinal fluid flow measurements at MR imaging. Radiology. 1996; 198:523–529. [PubMed: 8596861]
5. Bunck AC, Kroeger JR, Juettner A, Brentrup A, Fiedler B, Crelier GR, Martin BA, Heindel W, Maintz D, Schwindt W, Niederstadt T. Magnetic resonance 4D flow analysis of cerebrospinal fluid dynamics in Chiari I malformation with and without syringomyelia. European Radiology. 2012; 22:1860–1870. [PubMed: 22569996]
6. Bunck AC, Kroeger JR, Juettner A, Brentrup A, Fiedler B, Crelier GR, Martin BA, Heindel W, Maintz D, Schwindt W, Niederstadt T. Magnetic resonance 4D flow analysis of cerebrospinal fluid dynamics in Chiari I malformation with and without syringomyelia. Eur Radiol. 2012; 22:1860–1870. [PubMed: 22569996]
7. Bunck AC, Kroger JR, Juttner A, Brentrup A, Fiedler B, Schaarschmidt F, Crelier GR, Schwindt W, Heindel W, Niederstadt T, Maintz D. Magnetic resonance 4D flow characteristics of cerebrospinal fluid at the craniocervical junction and the cervical spinal canal. Eur Radiol. 2011; 21:1788–1796. [PubMed: 21404133]
8. Busch J, Giese D, Wissmann L, Kozerke S. Reconstruction of divergence-free velocity fields from cine 3D phase-contrast flow measurements. Magnetic Resonance in Medicine. 2013; 69:200–210. [PubMed: 22411739]
9. Canstein C, Cachot P, Faust A, Stalder AF, Bock J, Frydrychowicz A, Kuffer J, Hennig J, Markl M. 3D MR flow analysis in realistic rapid-prototyping model systems of the thoracic aorta: comparison with in vivo data and computational fluid dynamics in identical vessel geometries. Magn Reson Med. 2008; 59:535–546. [PubMed: 18306406]
10. Clarke EC, Fletcher DF, Stoodley MA, Bilston LE. Computational fluid dynamics modelling of cerebrospinal fluid pressure in Chiari malformation and syringomyelia. J Biomech. 2013; 46:1801–1809. [PubMed: 23769174]
11. Giese D, Haeberlin M, Barmet C, Pruessmann KP, Schaeffter T, Kozerke S. Analysis and correction of background velocity offsets in phase-contrast flow measurements using magnetic field monitoring. Magnetic Resonance in Medicine. 2012; 67:1294–1302. [PubMed: 21826731]
12. Ha H, Kim GB, Kweon J, Kim Y-H, Kim N, Yang DH, Lee SJ. Multi-VENC acquisition of four-dimensional phase-contrast MRI to improve precision of velocity field measurement. Magnetic Resonance in Medicine. 2015 n/a-n/a.
13. Hayashi N, Matsumae M, Yatsushiro S, Hirayama A, Abdullah A, Kuroda K. Quantitative Analysis of Cerebrospinal Fluid Pressure Gradients in Healthy Volunteers and Patients with Normal Pressure Hydrocephalus. Neurol Med Chir (Tokyo). 2015; 55:657–662. [PubMed: 26226976]
14. Heidari Pahlavian S, Bunck AC, Loth F, Shane Tubbs R, Yiallourou T, Kroeger JR, Heindel W, Martin BA. Characterization of the discrepancies between four-dimensional phase-contrast magnetic resonance imaging and in-silico simulations of cerebrospinal fluid dynamics. J Biomech Eng. 2015; 137:051002. [PubMed: 25647090]
15. Heidari Pahlavian S, Yiallourou T, Tubbs RS, Bunck AC, Loth F, Goodin M, Raisee M, Martin BA. The Impact of Spinal Cord Nerve Roots and Denticulate Ligaments on Cerebrospinal Fluid Dynamics in the Cervical Spine. PLoS ONE. 2014; 9:e91888. [PubMed: 24710111]
16. Helgeland A, Mardal KA, Haughton V, Reif BA. Numerical simulations of the pulsating flow of cerebrospinal fluid flow in the cervical spinal canal of a Chiari patient. J Biomech. 2014; 47:1082–1090. [PubMed: 24529910]

17. Hsu Y, Hettiarachchi HD, Zhu DC, Linninger AA. The frequency and magnitude of cerebrospinal fluid pulsations influence intrathecal drug distribution: key factors for interpatient variability. Anesthesia and Analgesia. 2012; 115:386–394. [PubMed: 22523420]
18. Hsu Y, Hettiarachchi HD, Zhu DC, Linninger AA. The Frequency and Magnitude of Cerebrospinal Fluid Pulsations Influence Intrathecal Drug Distribution: Key Factors for Interpatient Variability (vol 115, pg 386, 2012). Anesthesia and Analgesia. 2012; 115:879–879.
19. Iliff JJ, Wang M, Liao Y, Plogg BA, Peng W, Gundersen GA, Benveniste H, Vates GE, Deane R, Goldman SA, Nagelhus EA, Nedergaard M. A paravascular pathway facilitates CSF flow through the brain parenchyma and the clearance of interstitial solutes, including amyloid beta. Sci Transl Med. 2012; 4:147ra111.
20. Jacobs, PF.; Reid, DT.; Computer and A. S. A. o. SME. Rapid Prototyping & Manufacturing: Fundamentals of Stereolithography. Society of Manufacturing Engineers; 1992.
21. Jones CF, Lee JH, Kwon BK, Cripton PA. Development of a large-animal model to measure dynamic cerebrospinal fluid pressure during spinal cord injury: Laboratory investigation. J Neurosurg Spine. 2012; 16:624–635. [PubMed: 22519927]
22. Kress BT, Iliff JJ, Xia M, Wang M, Wei HS, Zeppenfeld D, Xie L, Kang H, Xu Q, Liew JA, Plog BA, Ding F, Deane R, Nedergaard M. Impairment of paravascular clearance pathways in the aging brain. Ann Neurol. 2014; 76:845–861. [PubMed: 25204284]
23. Ku JP, Elkins CJ, Taylor CA. Comparison of CFD and MRI flow and velocities in an in vitro large artery bypass graft model. Ann Biomed Eng. 2005; 33:257–269. [PubMed: 15868717]
24. Lagana MM, Chaudhary A, Balagurunathan D, Utriainen D, Kokeny P, Feng W, Cecconi P, Hubbard D, Haacke EM. Cerebrospinal fluid flow dynamics in multiple sclerosis patients through phase contrast magnetic resonance imaging. Curr Neurovasc Res. 2014; 11:349–358. [PubMed: 25233279]
25. Markl M, Bammer R, Alley M, Elkins C, Draney M, Barnett A, Moseley M, Glover G, Pelc N. Generalized reconstruction of phase contrast MRI: analysis and correction of the effect of gradient field distortions. Magnetic Resonance in Medicine. 2003; 50:791–801. [PubMed: 14523966]
26. Martin BA, Labuda R, Royston TJ, Oshinski JN, Iskandar B, Loth F. Spinal Subarachnoid Space Pressure Measurements in an In Vitro Spinal Stenosis Model: Implications on Syringomyelia Theories. Journal of Biomechanical Engineering-Transactions of the Asme. 132:2010.
27. Martin BA, Yiallourou TI, Pahlavian SH, Thyagaraj S, Bunck AC, Loth F, Sheffer DB, Kroger JR, Stergiopulos N. Inter-operator Reliability of Magnetic Resonance Image-Based Computational Fluid Dynamics Prediction of Cerebrospinal Fluid Motion in the Cervical Spine. Ann Biomed Eng. 2015
28. McCauley TR, Pena CS, Holland CK, Price TB, Gore JC. Validation of volume flow measurements with cine phase-contrast MR imaging for peripheral arterial waveforms. J Magn Reson Imaging. 1995; 5:663–668. [PubMed: 8748483]
29. Nelissen, RM. Fluid mechanics of intrathecal drug delivery. Citeseer; 2008.
30. Ong F, Uecker M, Tariq U, Hsiao A, Alley MT, Vasanawala SS, Lustig M. Robust 4D flow denoising using divergence-free wavelet transform. Magnetic Resonance in Medicine. 2015; 73:828–842. [PubMed: 24549830]
31. Pahlavian SH, Bunck AC, Loth F, Tubbs RS, Yiallourou T, Kroeger JR, Heindel W, Martin BA. Characterization of the Discrepancies between Four-Dimensional Phase-Contrast Magnetic Resonance Imaging and In-Silico Simulations of Cerebrospinal Fluid Dynamics. Journal of Biomechanical Engineering-Transactions of the Asme. 2015 In Press.
32. Papisov MI, Belov VV, Gannon KS. Physiology of the Intrathecal Bolus: The Leptomeningeal Route for Macromolecule and Particle Delivery to CNS. Mol Pharm. 2013
33. Silverberg G, Mayo M, Saul T, Fellmann J, McGuire D. Elevated cerebrospinal fluid pressure in patients with Alzheimer's disease. Cerebrospinal Fluid Res. 2006; 3:7. [PubMed: 16737542]
34. Simpson, K.; Baranidharan, G.; Gupta, S. Spinal Interventions in Pain Management. OUP Oxford; 2012.
35. Stadlbauer A, Salomonowitz E, Brenneis C, Ungersbock K, van der Riet W, Buchfelder M, Ganslandt O. Magnetic resonance velocity mapping of 3D cerebrospinal fluid flow dynamics in hydrocephalus: preliminary results. Eur Radiol. 2012; 22:232–242. [PubMed: 21863368]

36. Traber J, Wurche L, Dieringer MA, Utz W, von Knobelsdorff-Brenkenhoff F, Greiser A, Jin N, Schulz-Menger J. Real-time phase contrast magnetic resonance imaging for assessment of haemodynamics: from phantom to patients. Eur Radiol. 2015

37. Walker PG, Cranney GB, Scheidegger MB, Waseleski G, Pohost GM, Yoganathan AP. Semiautomated method for noise reduction and background phase error correction in MR phase velocity data. Journal of Magnetic Resonance Imaging. 1993; 3:521–530. [PubMed: 8324312]

38. Wostyn P, Audenaert K, De Deyn PP. More advanced Alzheimer's disease may be associated with a decrease in cerebrospinal fluid pressure. Cerebrospinal Fluid Res. 2009; 6:14. [PubMed: 19917128]

39. Yiallourou TI, Kroger JR, Stergiopulos N, Maintz D, Bunck AC, Martin BA. Comparison of 4D phase-contrast MRI flow measurements to computational fluid dynamics simulations of cerebrospinal fluid motion in the cervical spine. PLoS ONE. 2012; 7:e52284. [PubMed: 23284970]

40. Yiallourou TI, Kröger JR, Stergiopulos N, Maintz D, Martin BA, Bunck AC. Comparison of 4D Phase-Contrast MRI Flow Measurements to Computational Fluid Dynamics Simulations of Cerebrospinal Fluid Motion in the Cervical Spine. PLoS ONE. 2012; 7:e52284. [PubMed: 23284970]

41. Yushkevich PA, Piven J, Hazlett HC, Smith RG, Ho S, Gee JC, Gerig G. User-guided 3D active contour segmentation of anatomical structures: significantly improved efficiency and reliability. Neuroimage. 2006; 31:1116–1128. [PubMed: 16545965]

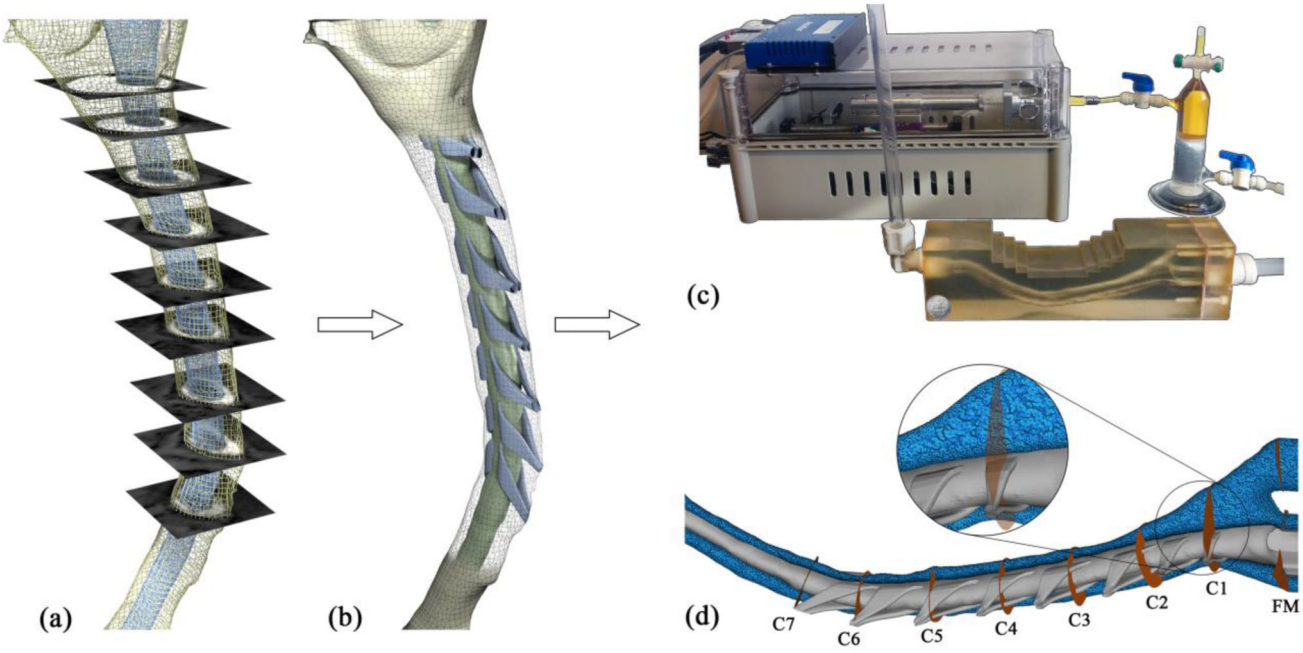

Figure 1.

Modeling process used to obtain the subject-specific geometry for CFD simulation and *in vitro* 4D Flow measurements. a) Reconstruction of the cervical SAS from MRI image segmentation. b) Addition of idealized dorsal and ventral nerve rootlets. c) Experimental platform including computer controlled pump, custom designed oil-water interface, and phantom 3D printed model. d) Computational grid used in the numerical simulation. Also, shown are the location of the axial planes on which the results were compared against in vitro 4D Flow.

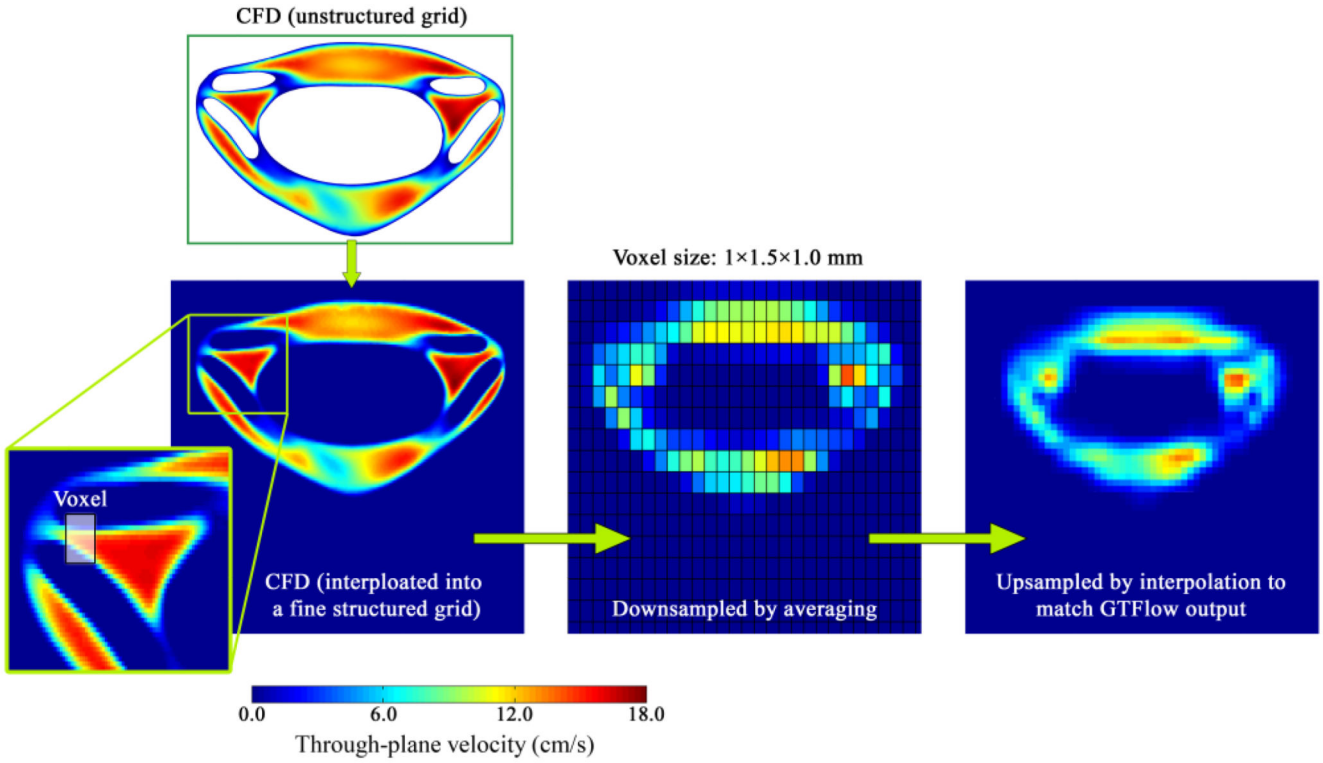

Figure 2.

Post-processing of the CFD velocities to match the 4D Flow output resolution: 1) Interpolation of the original CFD velocities onto a fine structured grid with the cell size equal to the smallest element in the unstructured grid. 2) Spatial averaging of CFD velocities from the fine structured grid onto a coarse structured grid with voxel size equal to the 4D Flow data. 3) Interpolation of the averaged data onto a fine structured grid with the same resolution as the 4D Flow data after post-processing in GTFlow software.

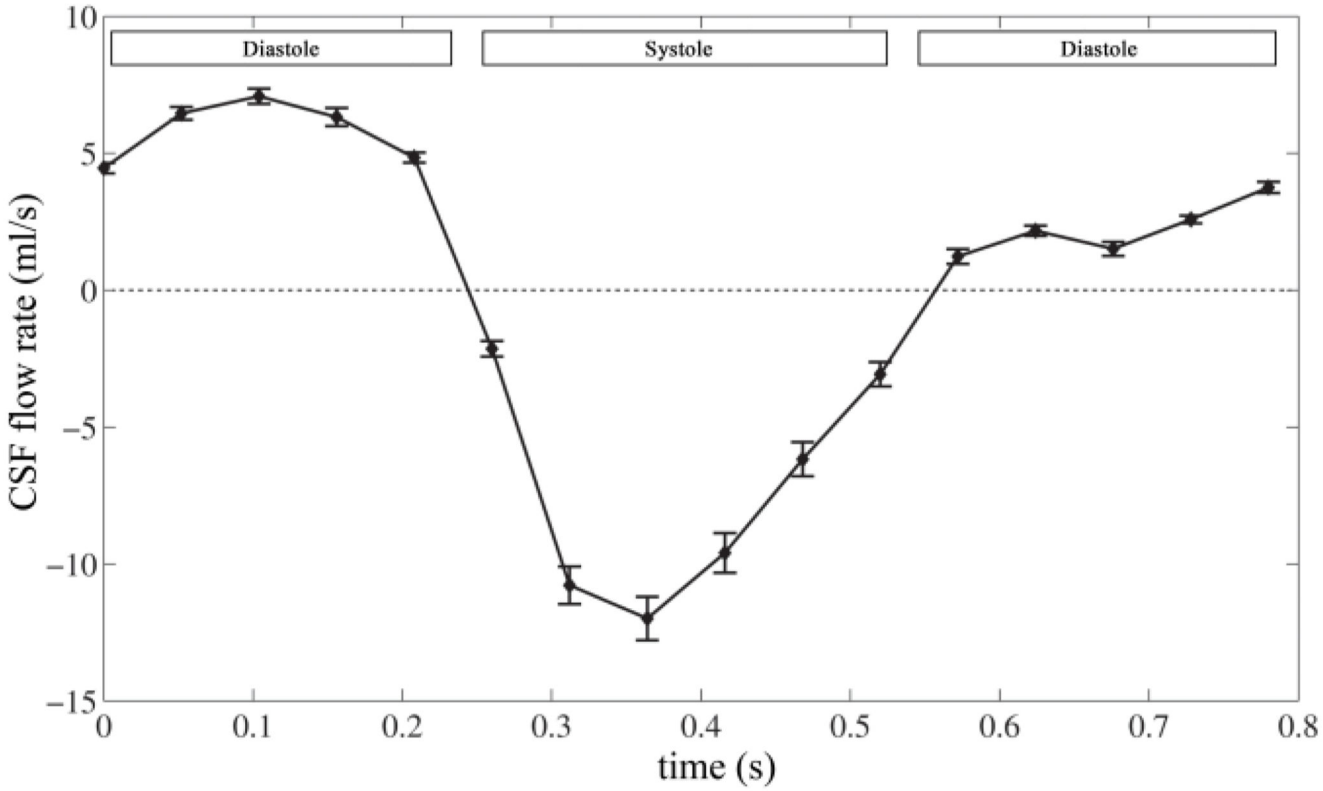

Figure 3.
Variation of CSF flow rates measured at different axial planes from 4D Flow. The average CSF flow rate was used as the inlet boundary condition for the CFD simulation.

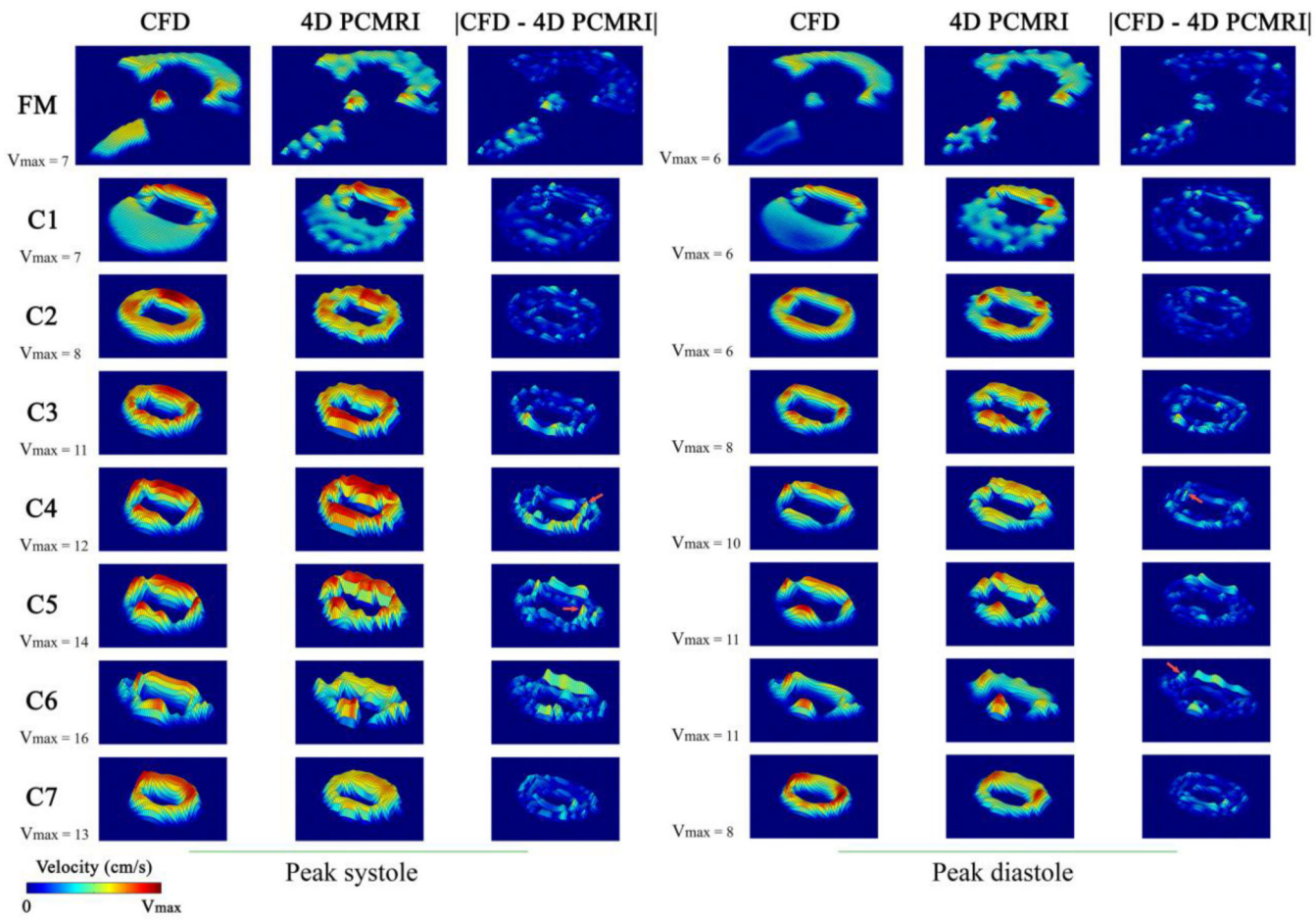

Figure 4.

Surface plot comparison of through-plane velocities simulated by CFD and measured by *in vitro* 4D Flow. Results are shown on eight different axial planes along the model (see Figure 1) and at the timeframes corresponding to peak systole (left) and peak diastole (right).

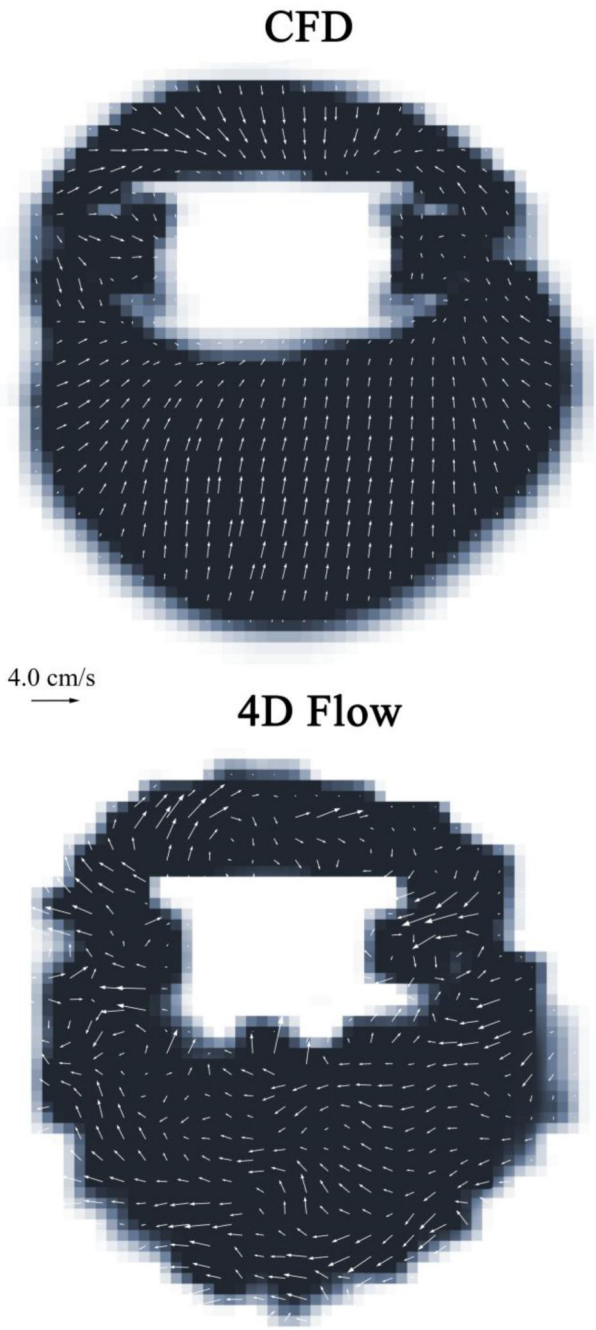

Figure 5.
Comparison of in-plane velocity vectors predicted by CFD and measured by 4D Flow plotted for a representative axial plane (C1) at the timeframe corresponding to peak systole.

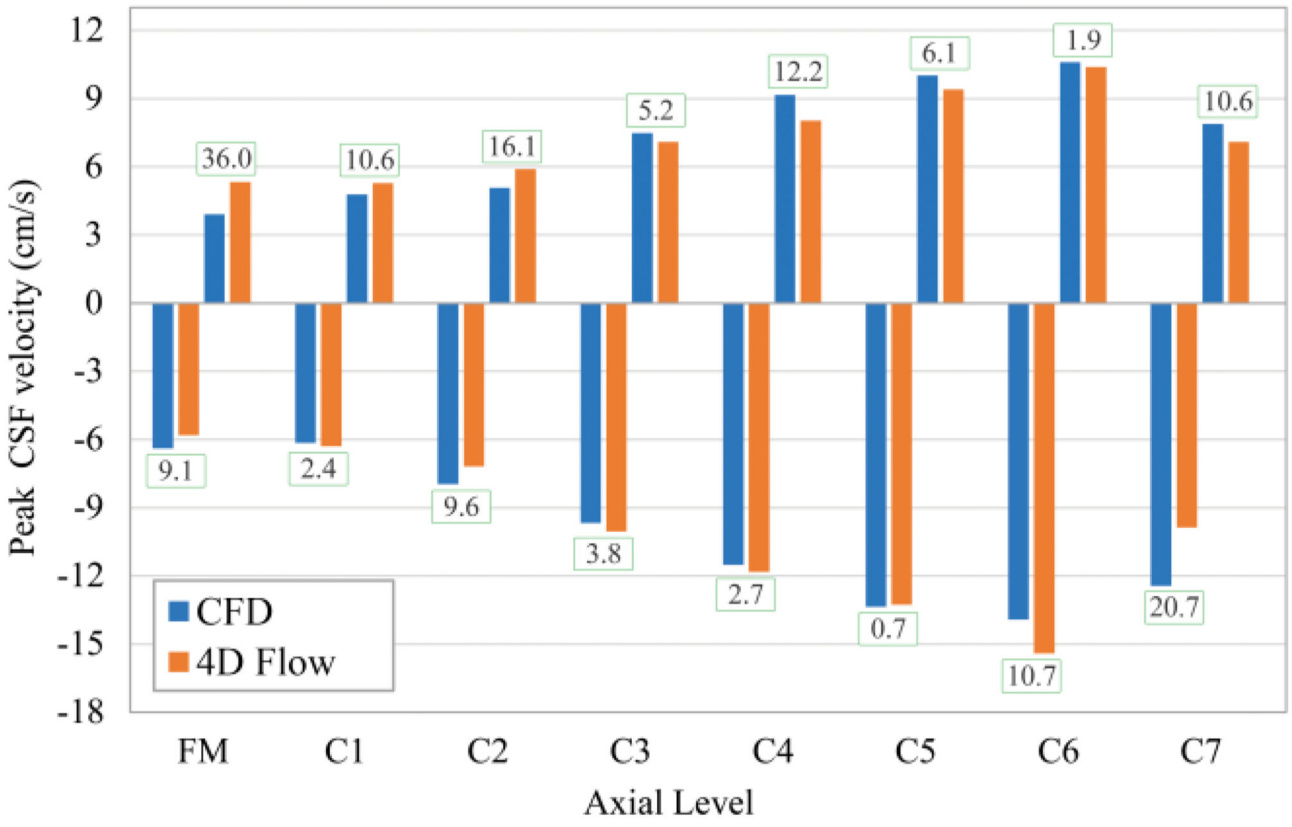

Figure 6.

Comparison of peak systolic (negative) and peak diastolic (positive) velocities obtained from CFD and 4D Flow at each axial plane. Percent difference for each comparison is shown in the adjacent box. Axial plane locations are shown in Figure 1.

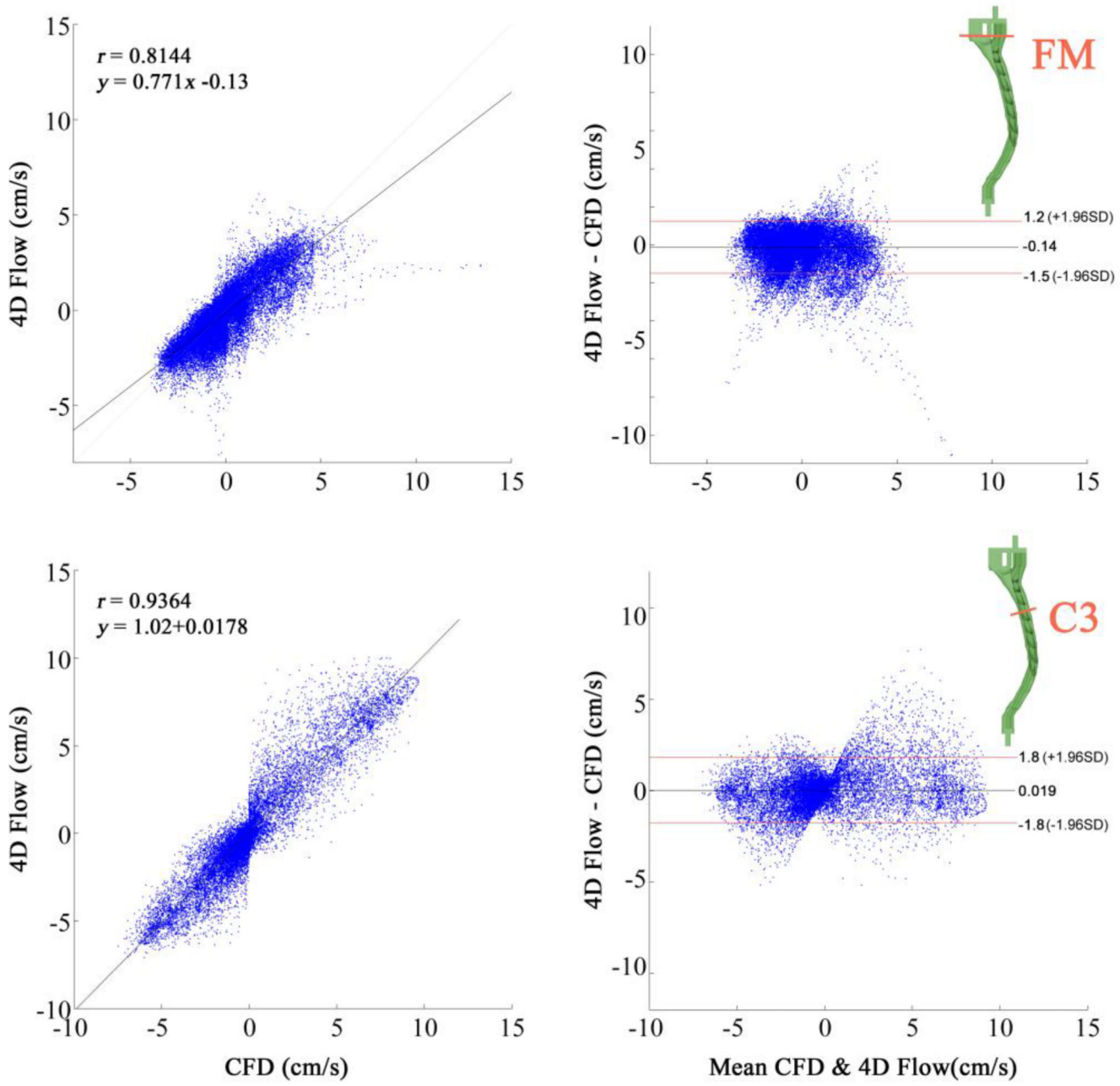

Figure 7.

Correlation and Bland-Altman plots between peak through-plane velocities predicted by CFD and measured by 4D Flow. The regression is shown in black solid line (left subplots) and the limit of agreement (95% confidence intervals) lines are shown in red (right subplots). Top pair: results from the axial plane with lowest correlation coefficient (FM). Bottom pair: results from the axial plane with the largest correlation coefficient (C3).

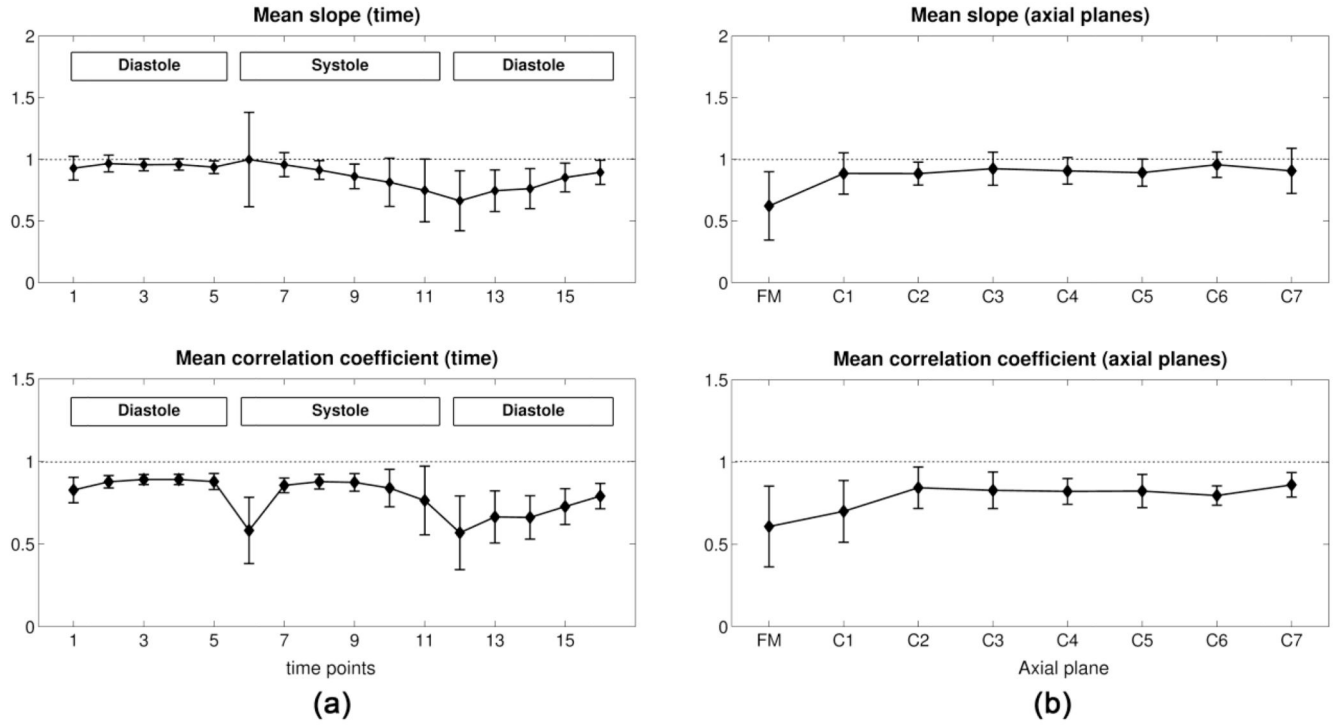

Figure 8.

Cumulative results of the correlation analysis for peak velocities obtained from CFD simulations and *in vitro* 4D Flow measurements. The linear regression analysis shown in Figure 6 was individually performed for each axial plane and timeframe. Results are summarized as mean slopes and correlation coefficients (r) of the fitted lines. a): Mean slopes and correlation coefficients averaged over all axial planes for all analyzed timeframes. b) Mean slopes and correlation coefficients averaged over all cardiac timeframes for all analyzed axial planes (FMC7). Systole and diastole corresponds to craniocaudal and caudocranial CSF flows, respectively.

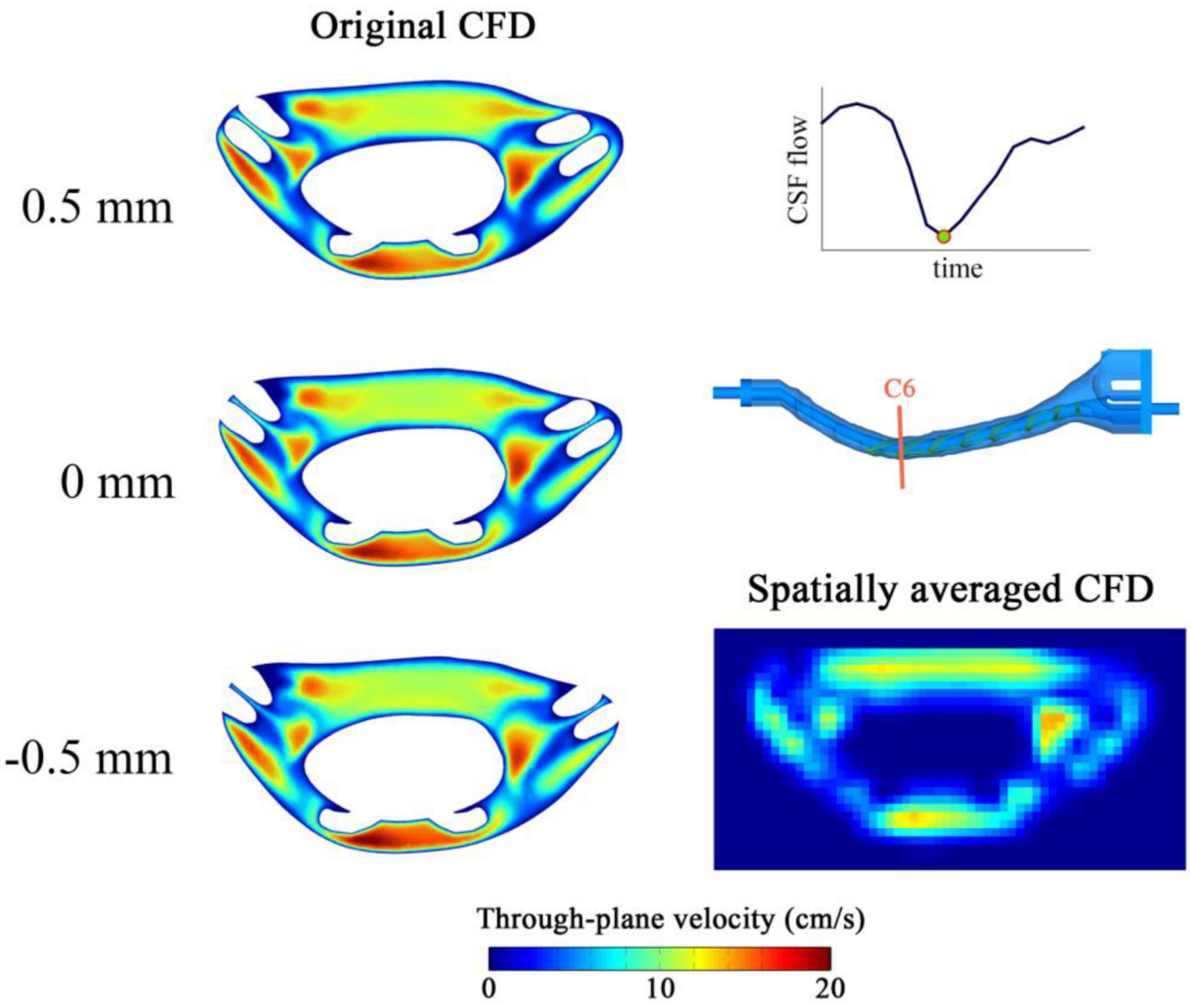

Figure 9.

Left) Variation of through-plane velocities obtained from the original CFD simulation over a distance of 1.0 mm (through-plane resolution of 4D Flow) near a representative axial plane (C6).The slices are 0.5 mm from one another with the slice labeled “0cm” corresponding to the axial location at which 4D Flow velocities were measured. Bottom right) Through-plane velocity distribution obtained from the averaged CFD results on the same axial plane.